IEICE TRANSACTIONS

on Electronics

DOI:10.1587/transele.2024ECP5022

Publicized:2024/08/28

This advance publication article will be replaced by the finalized version after proofreading.

A PUBLICATION OF THE ELECTRONICS SOCIETY

The Institute of Electronics, Information and Communication Engineers
Kikai-Shinko-Kaikan Bldg., 5-8, Shibakoen 3chome, Minato-ku, TOKYO, 105-0011 JAPAN

PAPER

Investigation of Equivalent Radiated Emissions of Photovoltaic Power Line Communications through Scaled Model

Yongzhe Wei [†,††], Zhongyuan Zhou [†,††a)], Zhicheng Xue [†,††], Shunyu Yao [†,††], and Haichun Wang [†,††], *Nonmembers*

SUMMARY Power line communication (PLC) technology utilizes the alternating current distribution network to transmit signals, enabling high-speed information exchange in photovoltaic (PV) power systems without the need for additional wiring, thereby saving costs. The use of PV PLC technology may potentially cause radiated emissions that interfere with wireless radiocommunications, consequently leading to electromagnetic compatibility issue. Additionally, conducting accurate radiated emission measurements on-site in PV power systems can be challenging. The paper proposes a methodology utilizing a scaled model for the equivalent radiated emissions of PV PLC. This approach facilitates the execution of equivalent testing for PV PLC radiated emissions under controlled laboratory conditions. Conducting a simulation study using CST to determine the equivalent simulation of actual long-line model through scaled short-line model, three scaled short-line models with different diameters were selected for comparison with the simulated radiated emission results of long-line model. After that, the optimal scaled short-line model was determined, followed by practical testing of the scaled short-line model in an anechoic chamber. Finally, by comparing the results, the accuracy of the simulation model was validated, this further substantiates the feasibility of the research methodology employed in this study. The study serves as a reference for achieving accurate prediction of PV PLC radiated emissions and the determination of associated limits in the future.

key words: *photovoltaic power system, power line communications, scaled model, radiated emission measurement*

1. Introduction

In recent years, photovoltaic (PV) power systems, serving as a green energy source, have been widely adopted worldwide [1]. PV power systems typically leverage existing power distribution grids to implement high-speed information exchange through power line communication (PLC) technology. PLC efficiently transmits electrical information data signals through the 380V/220V low-voltage power distribution network, eliminating the need for additional wiring, thereby saving costs [2]–[4]. The frequency bands for PLC technology vary across different countries and regions [5]–[7]. In China, the commonly used frequency band is 0.7 to 12 MHz [8]. Due to PLC employs the conventional power line as the transmission medium, which are designed for transmission of 50 Hz alternating current and are not shield, this could lead to potential interference with radiocommunications within the same frequency band during the operation of PLC [9], [10]. Therefore, it is particularly important to measure radiated emission from the PLC.

PLC employed in PV power systems concurrently utilizes two parallel conductors for signal transmission [11], [12]. The PLC signal current in the two conductors will flow in opposite directions with the same current intensity, known as differential-mode current. In this case, due to the opposite current directions, the electromagnetic fields generated by the two conductors can cancel each other out, resulting in a lower radiated field strength. However, in practical situations, the impedance unbalance in PLC systems can cause the current in the two conductors to transmit in the same direction, known as the common-mode current, this results in the power cables radiating a stronger electromagnetic field [2]. The equivalent circuit for the PLC current transmission model is shown in Figure 1. The blue lines represent the differential-mode current, while the red lines represent the common-mode current.

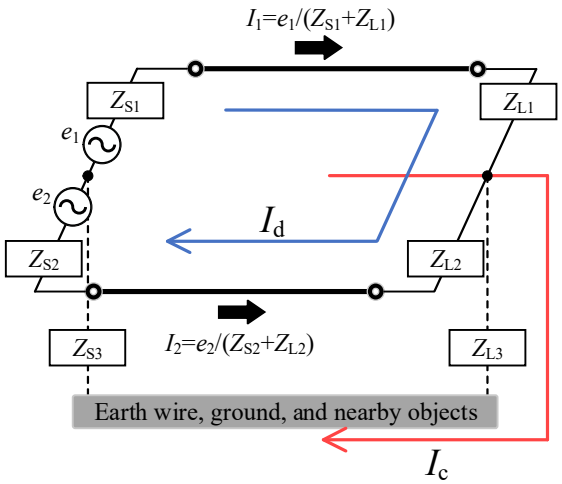

Fig. 1 Equivalent circuit of PLC current transmission model.

Where e_1 and e_2 represent the equivalent voltage sources of the PLC modem, The two phase lines convey equal-amplitude quadrature signals from the e_1 and e_2 to the load end. In addition , I_1 and I_2 denote the currents on the two phase lines, I_c is the common-mode current and I_d is the differential-mode current, Z_{S1}, Z_{S2}, and Z_{S3} respectively represent the impedance of the voltage sources and the ground impedance at the source end, Z_{L1}, Z_{L2}, and Z_{L3}

†The author are with the Research Center for Electromagnetic Environmental Effects, Southeast University, Nanjing ,211189 China.
††The author is with the Southeast University Suzhou Campus, Suzhou, 215123 China.
a) Email: zyzhou@seu.edu.cn

respectively represent the impedance of the loads connected to the phase lines and the ground impedance at the load end. It is important to note that the generation of I_c is due to the parasitic effects between the PLC equipment and the ground, as well as between the power lines and the ground. Here, impedance Z_{S3} and Z_{L3} are used to represent these parasitic effects.

By performing equivalent transformations on the PLC transmission model circuit, the value of I_c can be obtained through circuit simplification:

$$\begin{cases} I_c = \dfrac{Z_2 e_1 - Z_1 e_2}{Z_c \bullet Z_d} \\ Z_d = Z_1 + Z_2 \\ Z_c = \dfrac{Z_1 \bullet Z_2}{Z_1 + Z_2} + Z_3 \\ Z_i = Z_{Si} + Z_{Li} \left(i = 1,2,3\right) \end{cases} \tag{1}$$

Where Z_1 and Z_2 represent the sum of impedances on phase line 1, phase line 2, respectively, Z_3 represents the sum of the impedances to the ground. From the above calculations, it is evident that common-mode current exists in PLC systems lacking impedance match. This impedance imbalance often arises from unbalanced PLC modems (voltage sources e_1 and e_2, impedances Z_{S1} and Z_{S2}) and connected unbalance loads Z_{L1} and Z_{L2}.

The International Special Committee on Radio Interference (CISPR) has established the CISPR 11 standard, which specifies the limits for the radiated emission of industrial, scientific, and medical (ISM) equipment that unintentionally generates electromagnetic radiated emission [14]. However, CISPR 11 only provides conducted disturbance limits below 30 MHz and does not specify radiated field strength limits. Some standards specifically developed for PLC have been proven to have excessively stringent radiated emission limits[15], [16].Hence, some scholars have undertaken specific research on the radiated emissions measurement of PV PLC, demonstrating that testing PLC radiated emissions measurement is more meaningful than conducted emissions measurement [17]–[19], but the complexity of on-site testing conditions can lead to instability in the results of radiated emissions measurement. In laboratory conditions, a stable PLC radiation testing environment can be provided. The use of an anechoic chamber and antennas for radiated emission measurement of power cables is practical [20], [21]. However, most existing laboratory research focuses on in-house PLC radiation, where the in-house PLC line length is shorter and cabling is complex. Directly using in-house PLC for radiation testing is challenging to equivalent to the actual PV PLC outfield long line of radiation [13], [22], [23]. Therefore, it is important to find an equivalent testing for PV PLC radiated emission that can be conducted under laboratory conditions.

The paper proposes a methodology utilizing a scaled model for the equivalent radiated emissions of PV PLC, enabling effective testing of PLC radiated emissions equivalence under laboratory conditions. Based on the characteristics of power cable that can be equivalent to a series of dipole antennas, the antenna scaling model theory can be applied to transform the long-line configuration of PV PLC into a short-line model. This approach enables the feasibility of radiated emission testing under controlled laboratory conditions. The effectiveness of the scaled model is verified through CST simulation, and the scaled model is tested in laboratory conditions to validate the accuracy of the simulation results. This study serves as a reference for achieving accurate prediction of PV PLC radiative emissions and the determination of associated limits in the future.

2. Methods

2.1 Theory of PLC scaled model

The strategy for determining the radiation of power line is to divide the radiation structure into small electric dipole units. The electromagnetic field radiated by the entire cable is the sum of the electromagnetic fields generated by these basic dipole antennas [24]. Therefore, we can apply the scaled equivalent theory [25] to shrink the actual long-line PV cable by a certain proportion into a short-line model, enabling research under laboratory conditions. In the meanwhile, maintaining the electrical dimensions of the scaled short-line model consistent with the original long-line.

Suppose the frequency of the radiation issue for the original long-line is ω_1, with dielectric properties characterized by parameters ε_1 (dielectric constant), μ_1 (magnetic permeability), and δ_1 (electrical conductivity). The length is represented by r_1.and the electromagnetic field intensity vectors are E_1 and H_1. The Maxwell's equations are as follows:

$$\begin{cases} \nabla \times H_1 = j\omega_1 \bar{\varepsilon}_1 E_1 \\ \nabla \times E_1 = -j\omega_1 \mu_1 H_1 \end{cases} \tag{2}$$

In the equation (2), $\bar{\varepsilon}_1$ represents the complex dielectric constant of the medium for the original long-line radiation issue.

In the radiation issue of the scaled short-line model, the frequency is ω_2, with dielectric properties characterized by parameters ε_2 (dielectric constant), μ_2 (magnetic permeability), and δ_2 (electrical conductivity). The length is represented by r_2. And the electromagnetic field intensity vectors are E_2 and H_2. And then:

$$r_2 = k_1 r_1, \omega_2 = k_2 \omega_1, \bar{\varepsilon}_2 = k_3 \bar{\varepsilon}_1, \mu_2 = k_4 \mu_1 \tag{3}$$

The Maxwell's equations are as follows:

$$\begin{cases} \nabla \times H_2 = j\omega_2 \bar{\varepsilon}_2 E_2 \\ \nabla \times E_2 = -j\omega_2 \mu_2 H_2 \end{cases} \tag{4}$$

If we require the electromagnetic fields to be equal in the two radiation issues, i.e., $E_1 = E_2$ and $H_1 = H_2$, the

calculation can be deduced based on the two sets of Maxwell's equations as follows:

$$\begin{cases} \nabla \times H_1 = k_1 \bullet k_2 \bullet k_3 \bullet \left(j\omega_1 \bar{\varepsilon}_1 E_1 \right) \\ \nabla \times E_1 = k_1 \bullet k_2 \bullet k_4 \bullet \left(-j\omega_1 \mu_1 H_1 \right) \end{cases} \quad (5)$$

Let k_3 and k_4 be 1, i.e., maintaining the dielectric constant and magnetic permeability unchanged with frequency variation. Also, when the frequency increases by a factor of k, the length of the short line is reduced to $1/k$ of the original long line, i.e., $k_1=1/k_2$ ensuring that the electrical length remains constant. In this case, in Equation (5), $k_1 \bullet k_2 \bullet k_3 = 1$ and $k_1 \bullet k_2 \bullet k_4 = 1$ can be adjusted to ensure that the electromagnetic field distributions of the two radiation issues are consistent.

When the medium has losses (i.e., $\delta \neq 0$), or the electrical conductivity of the metal conductor in the antenna feeder is not approaching infinity, if it remains unchanged as the frequency increases by a factor of k, then δ should also increase by a factor of k, i.e., $\delta_2 = k\delta_1$. However, in general, achieving this is difficult. The core wire material of the power line used in PLC is often made of high-conductivity copper or aluminum, the radiated power far surpasses the dissipated power. Therefore, errors due to not increasing the electrical conductivity can be neglected [26]. The relationship between the parameters of the long-line and the scaled short-line is as shown in Table 1.

Table 1 Scaled short-line model parameter equivalent relationships.

Parameters	Long-line	Scaled short-line model	Parameters	Long-line	Scaled short-line model
Length	r	r/k	Dielectric constant	ε	ε
Frequency	f	kf	Magnetic permeability	μ	μ
Electrical conductivity	δ	$k\delta$	Excitation voltage	U	U/k

2.2 Radiated emission modeling and simulation of PLC scaled model

Based on the actual on-site investigation of a PV power station, the selected PLC power line model was denoted as ZC-YJLV22-0.6/1kV-3×185+1×95mm², i.e., a three-phase four-wire armored AC power line. The cross-section and composition of the cable model are shown in Figure 2. The dimensions and simulation parameters of each layer of the cable are provided in Table 2.

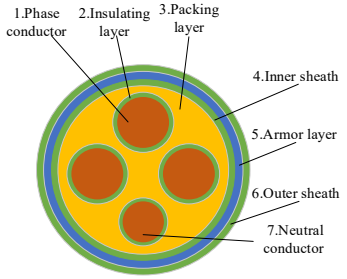

Fig. 2 Structure of the PLC Cable Model.

Table 2 Material Parameters for the PLC Cable Model

Structure of Each Layer of the Cable	Thickness (or Radius) (mm)	Material	Electrical conductivity (S/m)	Relative dielectric constant	loss angle tangent
1.Phase conductor	7.7 (Radius)	Al	3.7×10^7	——	——
2.Insulating layer	1.6/1.1	XLPE	——	2.3	0.008
3.Packing layer	——	PE	——	2.3	0.003
4.Inner sheath	2.0	PE	——	2.3	0.003
5.Armor layer	0.8	Steel	3.48×10^6	——	——
6.Outer sheath	1.8	PVC	——	3.2	0.1
7.Neutral conductor	5.5 (Radius)	Al	3.7×10^7	——	——

Establishing a PLC cable model in CST cable studio. The cross-section and composition of the cable model are shown in Figure 2. The dimensions and parameters of each layer of the cable align with the guidelines outlined in IEC 60502-1:2021 [27]. To validate the effectiveness of the scaled model and save simulation time, a single-direction long-line model with a practical line length of 25 meters was selected,16 meters above ground. Based on the equivalent circuit in Figure 1, choose two phase lines as the signal transmission lines, and construct the circuit model of the cables in the CST design studio.

With reference to the FCC Part 15 and its amendments, the regulations pertaining to radiated emissions measurement principles for Access Broadband over Power Line on overhead line installations were considered [28]. The arrangement of test positions is depicted in Figure 3. Initiate the calculation from the signal injection point on the power line in the longitudinal direction. Established measurement locations along the length of the power line at distances of 0, $\lambda/4$, and $\lambda/2$, where λ signifies the wavelength corresponding to the center frequency point of the PLC operating bandwidth. According to standard requirements, when conducting radiated emission measurement below 30 MHz, it is necessary to choose the vertical polarization direction for testing , the simulation settings were consistent with the standard requirements. The test distance under the long-line simulation was 30 m, the test distance was proportionally reduced when performing scaled short-line simulations.

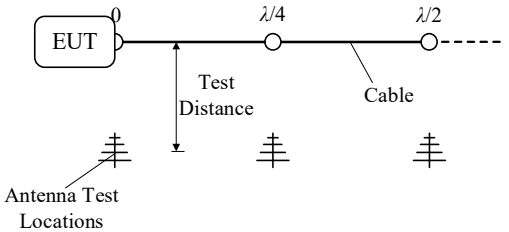

Fig. 3 PLC cable electric field test locations schematic diagram.

In practical PLC signal transmission, the utilization of orthogonal frequency division multiplexing (OFDM) technology is customary to address the issue of wastefulness

in spectrum resources [29]. According to practical usage scenarios, the frequency range of PLC signal transmission was determined to be 2~8 MHz . Due to the broadband nature of OFDM signals, actual test results are susceptible to additional out-of-band interference, making it challenging to accurately identify the measured signal. Therefore, a sinusoidal continuous wave signal within the range of 2~8 MHz was selected as the input excitation source for the simulation.

After determining the parameters for the actual long-line simulation model, investigate the selection of a scaled model with a ratio of 20:1 for scaled equivalent research. The variations in simulation parameters before and after scaling are presented in Table 3. In the actual radiated scenario, considering the aluminum core material of the AC cable, according to the previous analysis on the scaled model theory for PLC, the electrical conductivity can remain unaltered without undergoing scaling.

Table 3 Comparison of model parameters before and after scaling in PLC radiation simulation.

	Length (m)	Frequency (MHz)	Excitation voltage (V)	Simulation sampling points
Before scaling	25	2-8	1	1000
After scaling	1.25	40-160	0.05	1000

It is also important to note that the sampling points used in this simulation are identical before and after scaling. Although the frequency range increases after scaling and the frequency resolution is lower, the low resolution does not affect the accuracy of the simulation results. However, an excessive number of simulation sampling points would significantly increase the simulation time. Therefore, to conserve performance and reduce simulation time, this study uses the same sampling points before and after scaling.

The simulation of radiated emissions from the actual long-line PV PLC was conducted first, followed by the simulation of radiated emissions from the scaled short-line model. Considering practical measurement, addressing the scaling issue related to the cable diameter, the scaled short-line model was categorized into three types: proportional reduction of cable diameter, reduction to the standard cable diameter, and unchanged cable diameter. Radiated emission simulations were conducted for each type, further facilitating a comparison of differences among the three scaled short-line models. Specifically, the standard cable diameter chosen for scaling is model ZC-YJLV22-0.6/ 1kV-3×10+1×6mm² [27]. The cable structure and materials of each layer are consistent with the original long-line cable, with the dimensions of each layer detailed in Table 4.

Table 4 Dimensional parameters of the reduced to standard cable model

Structure of Each Layer of the Cable	Thickness (or Radius) (mm)	Structure of Each Layer of the Cable	Thickness (or Radius) (mm)
1.Phase conductor	1.8 (Radius)	5.Armor layer	0.2
2.Insulating layer	0.7	6.Outer sheath	1.8
3.Packing layer	——	7.Neutral conductor	1.4 (Radius)
4.Inner sheath	1.0		

2.3 Measurement setup

The verification experiments were conducted in the five-meter anechoic chamber at the school of mechanical engineering, Southeast University, Nanjing, China. The scaled short-line model was subjected to verification, and the arrangement of the test cables is depicted in Figure 4(a). At the signal injection end, a differential bridge was added to provide differential signals for the two phase lines, and a 50Ω load was set at the load end. The signal source(Keysight N9310A) was used , together with an EMI receiver (R&S ESI7) and a biconical antenna. The signal source emitted a swept signal in the range of 40 to 160MHz, and the receiver bandwidth was set to 100kHz. As the signal transmission frequency range for PV PLC actual long-lines is below 30MHz, to ensure the accuracy of the scaled model, the antennas were chosen in the vertical polarization direction for the verification experiments of the scaled model. The cable height and the testing position height were both set to 0.8m, as illustrated in Figure 4(b) at the test site.

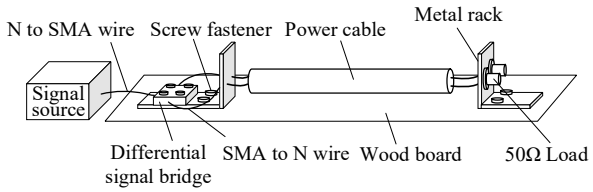

(a)

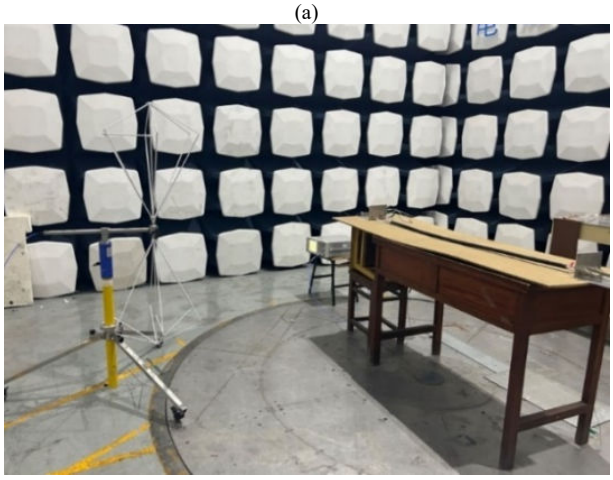

(b)

Fig. 4 (a) Arrangement of the scaled short-line model measurement for PLC, and (b) measurement in the anechoic chamber.

3. Result and Discussion

3.1 Comparison of simulation results between the long-line and scaled short-line models

Comparison of simulated electric field radiated emissions between the long-line and scaled short-line models is depicted in Figure 5. The simulated radiated field strength of the long-line model increases initially and then decreases with the rise in frequency, reaching its peak at 5.8 MHz . This phenomenon is attributed to the model's line length

being 25 meters, which is approximately half of the wavelength corresponding to the frequency of the maximum value at 5.8 MHz .

The average and maximum differences in simulated radiated field values between the long-line and scaled short-line models at various positions are presented in Table 5 and Table 6, respectively. Through comparison, it is evident that the radiated field strength results of the unchanged cable diameter model differ slightly from the long-line model, with some frequency points exhibiting differences exceeding 15 dB . As shown in Figure 5(c), when the test position is at $\lambda/2$ position, the unchanged cable diameter model reaches a maximum difference of 22.4 dB at 7.96 MHz (frequency range of the scaled short-line model: 159.3 MHz).

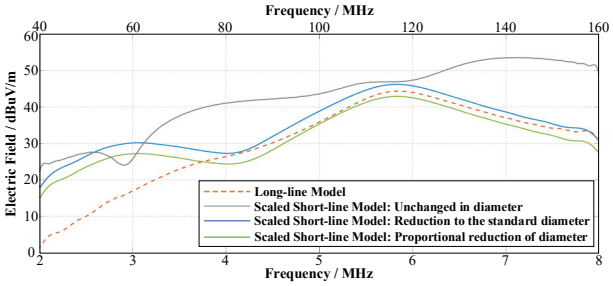

(a)

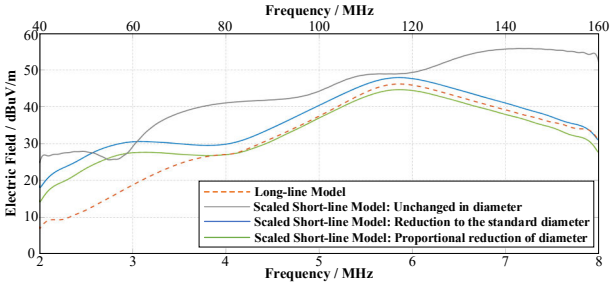

(b)

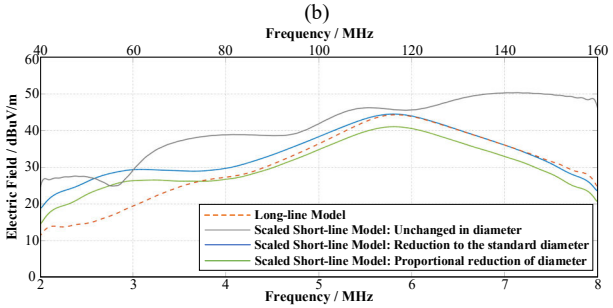

(c)

Fig. 5 (a) Comparison of electric field radiated emissions at the 0 position between the long-line and scaled short-line models, and (b) comparison of simulated results at the $\lambda/4$ position, and (c) comparison of simulated results at the λ/4 position at the $\lambda/2$ position.

Table 5 Comparison of the average difference in radiated electric field strength between the long-line and scaled short-line models.

	Unchanged in diameter	Reduction to the standard diameter	Proportional reduction of diameter
0 position	12.42 dB	4.85 dB	3.91 dB
$\lambda/4$ position	12.13 dB	4.62 dB	3.01 dB
$\lambda/2$ position	10.23 dB	3.25 dB	3.26 dB

Table 6 Comparison of the maximum difference in radiated electric field strength between the long-line and scaled-down models.

	Unchanged in diameter	Reduction to the standard diameter	Proportional reduction of diameter
0 position	21.76 dB	17.35 dB	14.19 dB
$\lambda/4$ position	22.26 dB	14.67 dB	11.35 dB
$\lambda/2$ position	22.41 dB	11.76 dB	8.30 dB

In the range of 2~3.4 MHz (frequency range of the scaled short-line model: 40~68 MHz), the field strength values and trends of the proportional reduction of diameter scaled model show slightly larger differences compared to the long-line model, as depicted in Figure 5(a), when the test position is at 0 position, the proportional reduction of diameter scaled model reaches a maximum difference of 14.19 dB at 2.26 MHz (frequency range of the scaled short-line model: 45.20 MHz). However, in the range of 3.4~8 MHz (frequency range of the scaled short-line model: 68~160 MHz), the trend is essentially consistent with the long-line model. The average difference within this range is only 1.74 dB. Despite some discrepancies at low frequencies. It can be learned from the data in Table 5, compared with the long-line model, the scaled short-line model of proportional reduction of diameter and reduction to the standard diameter have an error of less than 5 dB over the whole frequency band, which can meet the error requirements for engineering applications [30].

The reason for the discrepancies at low frequencies is that the test distances (30m for the long-line model and 1.5m for the scaled short-line model) fail to meet the distance requirements for the antenna's radiating region. Considering the PV PLC cable as a linear antenna, the field around the antenna is typically divided into the reactive near-field region, the radiating near-field region, and the far-field region based on the distance from the antenna [31]. At low frequencies, when the PLC cable length is small compared to the wavelength, it can be considered an electrically small antenna. In this case, the boundary between the reactive field and the radiating field is given by $R=\lambda/2\pi$. The testing distance of 30m used in this study, although exceeding the boundary of the reactive near-field region, is still relatively close to it. Due to the influence of the reactive field, the electromagnetic field distribution becomes complex, resulting in significant differences in radiated emission results before and after scaling in the low-frequency range. At high frequencies, due to the shorter wavelength, the PLC cable can be considered an electrically large antenna. The boundary distance of the reactive near-field region for an electrically large antenna is depicted as equation (6), and the boundary distance of the radiating near-field region is represented by equation (7)[32].

$$R_1 = \sqrt{\frac{2}{3\sqrt{3}}\left(\frac{L^3}{\lambda}\right)} \approx 0.62\sqrt{\frac{L^3}{\lambda}} \tag{6}$$

$$R_2 = \frac{2L^2}{\lambda} \tag{7}$$

Where R_1 represents the boundary distance of the reactive near-field region for an electrically large antenna,

R_2 represents the boundary distance of the radiating near-field region, L represents the maximum length of the antenna, and λ represents the wavelength. At high frequencies, the 30m testing distance is located in the far-field region, where the reactive field has almost no impact on the radiating field. Therefore, the consistency of the radiated emission results before and after scaling is relatively good. It is also important to note that while theoretical conditions delineate distance criteria for field regions, in practice, the characteristics of fields do not change abruptly but rather gradually. Thus, it can be observed that from low frequency to high frequency, the differences in radiated emission results before and after scaling gradually reduce, eventually stabilizing.

Meanwhile, the CPU time consumed for simulation solving by the scaled short-line model and the long-line model is 188s and 338s, respectively. This indicates that the scaled short-line model, while effectively representing the long-line radiation emission, also saves computation time. This provides a convenient approach for estimating radiation emissions of cables with complex structures in the future. The computer used in this article: CPU, Intel Xeon Gold 6154, GPU, NVIDIA GeForce RTX 3080 Ti, RAM, 64 GB.

Reduction to the standard cable diameter scaled model, the cable cross-sectional area was determined according to the standard as 10 mm² for the phase wire and 6 mm² for the neutral wire, slightly larger than the 9.25 mm² and 4.75 mm² of the proportional reduction of diameter scaled model. From the graph, it can be observed that the field strength variation trends of the two models are basically consistent, but the radiated field strength values are slightly higher than the proportional reduction of diameter scaled model.

The comparison of the differences in radiated electric field strength between the three scaled models and the long-line model is illustrated in Figure 6. From the simulation results, it is evident that the proportional reduction of diameter scaled model exhibits the best fitting with the long-line model, confirming the effectiveness of the scaled model. Considering the practical cable selection during measurement, although the fitting accuracy of the reduction to the standard diameter scaled model is not as high as that of proportional reduction of diameter scaled model, the two models show a generally consistent trend. Moreover, when compared to the long-line model, the average difference in simulated radiated field strength within the tested frequency range is 4.2dB. Therefore, in the measurement and validation phase, the choice was made to use the reduction to the standard diameter scaled model for comparative analysis of PLC radiation.

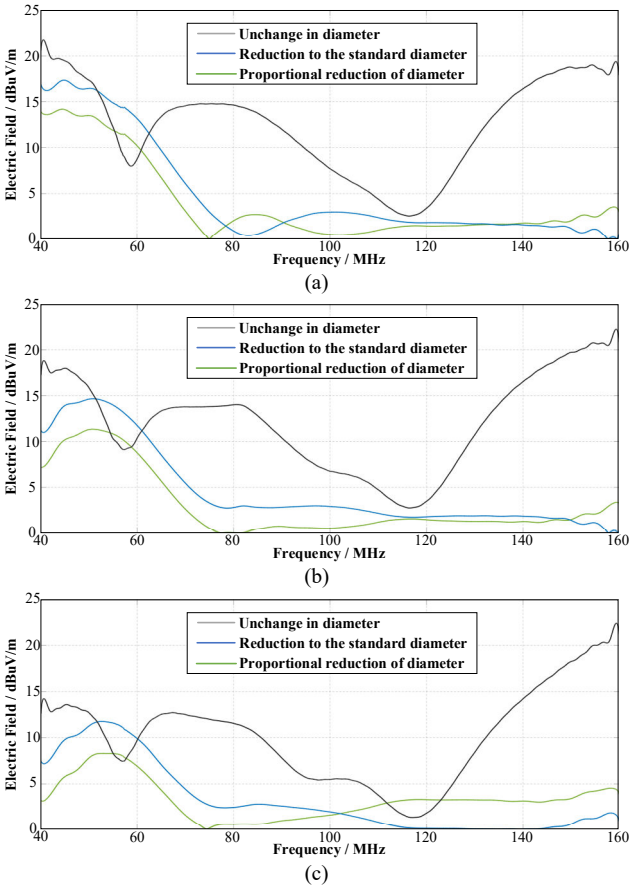

Fig. 6 (a) The difference in radiated field strength between the long-line and scaled short-line models at 0 position, and (b) the difference in radiated electric field strength at $\lambda/4$ position, and (c) the difference in radiated electric field strength at $\lambda/2$ position

From the simulation results, it is evident that the radiation results of the scaled short-line model with an unchanged diameter exhibit a lower fitting accuracy with the long-line model. However, its trend and numerical values still possess certain reference value. In cases where the scaling factor is relatively large or the diameter of the long-line model is small, it may be appropriate to consider using a short-line model that only changes the length for simulation and measurement studies. Additionally, the introduction of a correction factor for the radiation results of the short-line model can be considered for accurate prediction of the long-line model's radiation results.

3.2 Comparison of simulation results and measurement results for the scaled model

To validate the accuracy of the equivalent long-line radiation from the scaled short-line model, validation experiments were conducted. The scaled short-line model with reduced diameter to the standard cable was chosen for the comparative simulation results. The cable used in the experiment had the model number " ZC-YJLV22-0.6/1kV-3×10+1×6mm²", The specific dimensional parameters are shown in Table 4. Taking the half-wavelength ($\lambda/2$) position

as an example for the comparative simulation and measurement results, the illustration in Figure 7 shows the solid line represents the simulation results and the dotted line represents the measurement validation results. The results indicate that the simulated results of the scaled short-line model align well with the measurement results, with an average difference of 2.91 dB, confirming the accuracy of the simulation model. This further validates the credibility of the method using scaled models to investigate actual long-line PLC radiated emission measurement.

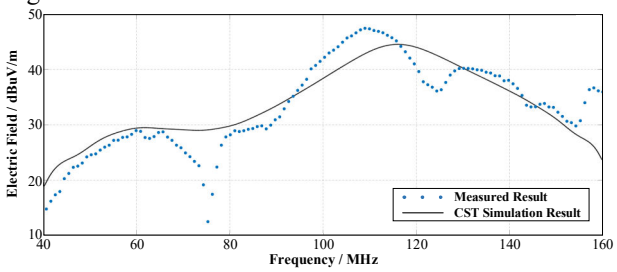

Fig. 7 Comparison of PLC scaled short-line model radiated emission simulation and measurement results.

However, it should be noted that, in comparison to the simulation results, there are noticeable discrepancies at certain frequency points in the test results, manifesting phenomena such as resonance frequency drift and an increase in resonances. The occurrence of these situations may be attributed to factors such as object scattering in the laboratory and assembly errors in the test setup. Due to the absence of precision cutting equipment, the experimental arrangement does not qualify as precise measurements for simulating the model [33].The remaining differences could be attributed to two factors. Firstly, the finite number of simulations and measurements may not be sufficient to achieve the best match. Secondly, the measurement uncertainty also has a certain impact [34],[35]. Further research will delve further into the measurement uncertainty and the unbalance of the cable.

The above analysis demonstrates that the scaled model can be applied to radiated emission testing of PV PLC cables under laboratory conditions. However, when dealing with excessively long cables requiring a larger scaling ratio, additional considerations may be necessary. Firstly, a larger scaling ratio means that the cross-sectional area of the scaled cables also needs to be smaller. During practical testing, it is crucial to consider whether smaller cross-sectional cables are commercially available for use. According to standards, it is recommended that the minimum cross-sectional area of cables should not be less than 1.5mm²[27]. Secondly, a larger scaling ratio also implies a broader frequency range after scaling. As the frequency increases, the required test distance decreases. When a larger sized antenna is close to the test cable, the loading effect of the antenna during the measurement may disrupt the field distribution, resulting in inaccurate measurement results. Therefore, it is necessary to consider selecting appropriately sized receiving antennas to ensure the accuracy of the measurements.

4. Conclusion

The paper proposes a methodology utilizing a scaled model for the equivalent radiated emissions of PV PLC, enabling effective testing of PLC radiated emissions equivalence under laboratory conditions. Based on the characteristics of power cable that can be equivalent to a series of dipole antennas, the antenna scaling model theory can be applied to transform the long-line configuration of PV PLC into a short-line model. This approach enables the feasibility of radiated emission measurement under controlled laboratory conditions. Selecting three scaled short-line models with different diameters, a comparison of simulated radiated emission results was conducted in CST with the long-line model to verify the effectiveness of the scaled models. Subsequently, a scaled short-line model of PV PLC was constructed in the anechoic chamber for on-site validation measurement. The results indicate that the scaled short-line simulation model is accurate. This further validates the credibility of the method using scaled models to investigate actual long-line PLC radiated emissions measurement, further research will delve further into the measurement uncertainty and the unbalance of the cable. This study serves as a reference for achieving accurate prediction of PV PLC radiated emissions and the determination of associated limits in the future.

References

[1] REN21, “Renewables Global Status Report,” 2023. https://www.ren21.net/reports/global-status-report/

[2] S. Sakuta, Y. Watanabe, M. Tokuda, and T. Higuma, “Terminal Condition Dependency of Transmission Characteristics for High-speed Power Line Communication,” 2007 IEEE Int. Symp. Electromagn. Compat., Honolulu, USA, pp.668-673, Jul. 2007. DOI:10.1109/isemc.2007.131

[3] N. Kuwabara , T. Matsushima , and Y. Fukumoto , “Method of implementing radiation resistance to analysis model for radiated emission using chain parameter matrix,” IEICE Commun. Express, vol.9, no.9, pp.446-450, 2020. DOI:10.1587/comex.2020XBL0070

[4] D. Righini , F. Passerini , and A. M. Tonello , “Modeling Transmission and Radiation Effects When Exploiting Power Line Networks for Communication,” IEEE Trans. Electromagn. Compat., vol.60, no.1, pp.59-67, 2017. DOI:10.1109/ TEMC.2017.2728370

[5] European Committee for Electrotechnical Standardization, “CENELEC-EN 50065-1,” 2011. https://www.cencenelec.eu/

[6] European Telecommunications Standards Institute, “ETSI-TS 101867,” 2000. https://www.etsi.org

[7] A. Mengi , M. Waechter , and M. Koch , “500 kHz G3-PLC access technology for the roll-outs in Germany,” 18th IEEE ISPLC, Glasgow, UK, pp.179-183, Mar. 2014. DOI: 10.1109/ isplc.2014.6812358

[8] Huawei, “PLC-IoT Industry Development White paper,” 2021. https://e.huawei.com/cn/material/networking/.

[9] S. Battermann and H. Garbe , “ Influence of PLC transmission on the sensitivity of a short-wave receiving station,” 9th IEEE ISPLC, Vancouver, Canada, pp.224-227, APR. 2005. DOI:10.1109/isplc. 2005.1430501

[10] J. Wu, Q. Guo, C. Yue, L. Xie, and C. Zhang, “Special Electromagnetic Interference in the Ionosphere Directly Correlated With Power System,” IEEE Trans. Electromagn. Compat., vol.62,

no.3, pp.947-954, 2020. DOI:10.1109 /TEMC. 2019.2918280

[11] H. Okumura, T. Matsushima, N. Kuwabara, T. Yamamoto, T. Wakisaka, and Y. Fukumoto, “Experimental study of the relationship between maximum common mode current and maximum magnetic field strength using a simple power distribution line model,” IEICE Commun. Express, vol.8, no.5, pp.178-183, 2020. DOI:10.1587/ comex.2019XBL0004

[12] N. Kuwabara, T. Matsushima, Y. Fukumoto, and H. Okumura, “Characteristics of Radiated Emission by PLC Signal from Three-wire Power Cable,” 2019 IEEE Int. Symp. Electromagn. Compat. - EMC EUROPE , Barcelona, Spain, pp.262-272, Sept. 2019. DOI:10.1109/ emceurope.2019.8872015

[13] T. Matsushima, H. Okumura, N. Kuwabara, and Y. Fukumoto, “Imbalance difference model for prediction of unintentional radiated emission from 10-wire power cable using for power line communication,” Wireless Networks, 2020. DOI:10.1007/s11276-020-02475-0

[14] International special committee on radio interference, “CISPR 11:2015,” 2015. https://www.iec.ch/

[15] UK Radio Communications Agency, “MPT 1570,” 2003.

[16] D. Hansen, “Review of EMC aspects in recent European PLC development,” 2002 IEEE Power. Engn. Soc. Summer Meeting , Chicago, USA, pp.1200-1216, Jul. 2002. DOI:10.1109/ PESS.2002. 1043488

[17] S. Linder and K. Wiklundh, “In-situ Measurements of Conducted and Radiated Emissions from Photovoltaic Installations,” 2022 IEEE Int. Symp. Electromagn. Compat. - EMC EUROPE, Gothenburg, Sweden, pp.231-236, Sept. 2022. DOI:10.1109/EMCEUROPE 51680.2022.9901001

[18] J. Andersson, H. Olsson, and A. Theocharis, “Analysis of electromagnetic compatibility in photovoltaic installations validated by site measurements,” 14th IEEE POWERTECH , Madrid, Spain, Jun. 2021. DOI:10.1109/PowerTech46648.2021. 9494791

[19] G. Singh, E. Auel, J. Owens, T. Cooke, M. Stephens, and W. Howe, “Detection of High Frequency Conducted Emission using Radiated Fields,”10th IEEE ISGT-EUROPE, The Hague, Netherlands, pp. 334-338, Oct. 2020.

[20] J. Jia, D. Rinas, and S. Frei, “Predicting the Radiated Emissions of Automotive Systems According to CISPR 25 Using Current Scan Methods,” IEEE Trans. Electromagn. Compat., vol.58, no.2, pp.409-418, 2015. DOI:10.1109/ TEMC.2015.2511185

[21] G. H. Li, W. Qian, A. Radchenko, J. P. He, G. Hess, R. Hoeckele, T. Van Doren, D. Pommerenke, and D. Beetner, “ Prediction of Radiated Emissions From Cables Over a Metal Plane Using a SPICE Model,” IEEE Trans. Electromagn. Compat., vol.57, no.1, pp.61-68, 2015. DOI:10.1109/ TEMC.2014.2364405

[22] T. Matsushima, H. Okumura, N. Kuwabar, M. Iwasaki, D. Koike, an d Y. Fukumoto, “Investigation of Multi-Cable Effect to Radiated Emission from Cable Used for Power Line Communication,” 2020 IEEE Int. Symp. Electromagn. Compat. - EMC EUROPE, Rome, Italy, Sept. 2020. DOI:10.1109/emceurope48519.2020. 9245704

[23] T. Yamamoto, H. Okumura, T. Wakisaka, T. Matsushima, N. Kuwabara, and Y. Fukumoto, “Calculation of Electromagnetic Field Radiated from Power Line Communication of Three Wires System,” 2019 IEEE Int. Symp. Electromagn. Compat. - EMC Sapporo/APEMC, Sapporo, Japan, pp.704-707, Jun. 2019. DOI: 10.23919/EMCTokyo.2019.8893771

[24] A. Liakouti, A. Benbassou, C. Pasquier, C. Faure, K. E. Drissi, and F. Paladian, “Closed form model of radiated EM field from wired systems and analysis of coupling impact,” 2017 IEEE Int. Symp. Electromagn. Compat. - EMC EUROPE, Angers, France, Sept. 2017 .DOI: 10.1109/EMCEurope.2017.8094733

[25] A. Piantini, J. M. Janiszewski, A. Borghetti, C. A. Nucci, and M. Paolone, “A scale model for the study of the LEMP response of complex power distribution networks,” IEEE Trans. on Power Delivery, vol.22, no.1, pp.710-720, 2007.DOI:10.1109/TPWRD. 2006.881410

[26] W. Yan, J. Yu, D. C. Yu, and K. Bhattarai, “A new optimal reactive power flow model in rectangular form and its solution by predictor correct or primal dual interior point method ,” IEEE Trans. on Power Systems . vol.22, no.1 pp.61-67, 2006. DOI:10.1109/ TPWRD.2006.881410

[27] International Electrotechnical Commission, “IEC 60502-1:2021,” 2021. https://www.iecee.org/.

[28] Federal Communications Commission, “FCC Part 15,”2024. https://www.ecfr.gov/.

[29] A. Omri, J. H. Fernandez, and R. Di Pietro, “Extending device noise measurement capacity for OFDM-based PLC systems: Design, implementation, and on-field validation,” Computer Networks, vol.237, 2023. DOI: 10.1016/j.comnet.2023.110038

[30] J. He, X. Li, S. Tao, L. Cao, and X. Wang, “Electromagnetic Radiation Mechanism Analysis and Field Strength Prediction of an Elementary Digital Inverter with Cables,” Chinese Journal of Electrical Engineering, vol.8, no.3, pp.37-48, 2022.

[31] IEEE, "IEEE Std 145-2013-IEEE Standard for Definitions of Terms for Antennas,"2014. DOI: 10.1109/IEEESTD.2014.6758443.

[32] S. Zhong, Antenna Theory and Techniques Second Edition, Publishing House of Electronics Industry, Beijing, 2015

[33] D. Campos, K. M. G. Santos, D. J. C. Pereira, P. A. Santos, L. S. Ribeiro, and T. M. Silveira, “Analysis and Validation of a Computational Model for a Two Bipolar Drain Wire Cables,” 7th BTSym - Emerging Trends and Challenges in Technology , Campinas, Brazil ,vol.207, pp.623-629, Nov. 2021. DOI:10.1007/ 978-3-031-04435-9_67

[34] S. Sun, G. Liu, J. L. Drewniak, and D. J. Pommerenke, “Hand-Assembled Cable Bundle Modeling for Crosstalk and Common-Mode Radiation Prediction,” IEEE Trans. Electromagn. Compat., vol.49, no.3, pp.708-718, 2007. DOI:10.1109/TEMC. 2007.897142

[35] G. Andrieu, A. Reineix, X. Bunlon, G. Andrieu, J. P. Parmantier, L. Kone, and B. Demoulin, “Extension of the ‘Equivalent Cable Bundle Method’ for Modeling Electromagnetic Emissions of Complex Cable Bundles,” IEEE Trans. Electromagn. Compat., vol.51, no.1, pp.108-118,2009. DOI: 10.1109/TEMC.2008.2007803

Yongzhe Wei received the M.S. degree in agricultural engineering from Northwest A&F University, Yangling, China in 2022. He is currently working toward the Ph.D. degree in Southeast University, Nanjing, China. His current research interests include the electromagnetic compatibility and measurement instrumentation.

Zhongyuan Zhou received the M.S. and Ph.D. degrees in mechatronic engineering from Southeast University, Nanjing, China, in 1998 and 2008, respectively. He is currently a Professor with the Research Center for Electromagnetic Environmental Effects, School of Mechanical Engineering, Southeast University. His main research interests include electromagnetic compatibility and electromagnetic environmental effects.

ZhiCheng Xue received the B.S. degree in mechanical engineering from Zhengzhou University , Zhengzhou, China in 2022. He is currently working toward the Ph.D. degree in Southeast University, Nanjing, China. His current research interests include the electromagnetic compatibility and measurement instrumentation.

Shunyu Yao received the M.S. degree in electronic communications and computer engineering from the University of Nottinghan, UK. He is currently working toward the Ph.D. degree in Southeast University, Nanjing, China. His current research interests include the electromagnetic compatibility and development of electric field probe.

Haichun Wang received the B.S. degree in mechanical engineering from Southeast University, Nanjing, China in 2022. She is currently working toward the Ph.D. degree in Southeast University, Nanjing, China. Her current research interests include the electromagnetic compatibility measurement techniques.